

CFD FOR SUPERSONIC GAS PROCESSING

Bart PRAST, Bart LAMMERS and Marco BETTING

Twister BV, Einsteinlaan 10, 2289 CC, Rijswijk, NETHERLANDS

ABSTRACT

An improved version of the Twister™ Supersonic Gas separator concept was tested in Gasunie Research Laboratories in the Netherlands during 2005 and 2006 in a closed loop test facility using a multiphase pump. Advanced CFD models were used to improve the internal design of the Twister separator, leading to a new design with a reduced overall pressure drop. The most important aim of the experimental work was to verify CFD model calculations of pressure drop and component recovery performance. In this paper the CFD model used for the prediction of the results is described. The results of one experiment are compared with the results from CFD.

NOMENCLATURE

| | |
|-------------|---|
| c | speed of sound |
| D_k | binary diffusion coefficient of component k |
| k_B | Boltzmann constant |
| m_n | mass of a vapour molecule of the nucleating component |
| m_v | mass of a vapour molecule |
| N_A | Avogadro's constant |
| N_{comp} | The number of condensable vapours in the mixture |
| n_{Lk} | liquid molar density of component k |
| n_{vk} | vapour molar density of component k |
| p | pressure |
| r^* | critical cluster size |
| R_v | specific gas constant |
| u | velocity |
| u_j | velocity component |
| u_{jd} | drift velocity component |
| Nu_{mk} | Nusselt number for mass transfer for component k |
| S | Saturation ratio |
| Sc_t | turbulent Schmidt number |
| S_k | Saturation ratio of component k |
| T | temperature |
| W_k | molar mass of component k |
| y_k | molar fraction of component k |
| y_{eqvk} | equilibrium molar fraction of component k |
| Y_{vk} | vapour mass fraction of component k |
| Y_{Lk} | liquid mass fraction of component k |
| Y_{nN} | liquid mass fraction of nucleating component |
| γ | isentropic expansion factor |
| μ_{JT} | Joule-Thomson coefficient |
| μ | dynamic viscosity |
| μ_t | turbulent viscosity |
| ρ | density |
| ρ_v | vapour density |
| ρ_L | liquid density |
| ρ_{Lk} | liquid density of component k |

ρ_{Ln} liquid density of the nucleating component
 σ surface tension

INTRODUCTION

The Twister™ is a novel gas dew pointing device in which natural gas flows through a separation section at supersonic velocity. The Twister device is used to remove condensable vapours such as water or natural gas liquids (NGL) from a gas stream in order to lower the (water) dewpoint of the gas or strip the gas of heavy hydrocarbons which can generate additional revenue.

The three main physical processes in Twister™ are:

- A near isentropic expansion resulting in a low temperature and pressure due to the high (supersonic) velocity.
- Non-equilibrium condensation of vapours resulting in a fine mist of sub-micron sized droplets.
- Separation by inertia of droplets heavier than the surrounding gas due to a strong swirling flow.

Although the application of the combination of these processes is new, the physics behind the individual processes have been known for some time.

Supersonic flows have been studied mainly in aeronautical applications since the 19th century. Ernst Mach (1838-1916) was the first to recognize the dependency of the aerodynamic behaviour on the ratio u/c . He was also the first to note the sudden and discontinuous changes (gas dynamic shock waves) in the behaviour of an airflow when the ratio u/c , indicated by the Mach number, goes from being greater than 1 (supersonic) to less than 1 (subsonic).

As viscous and heat conduction effects are normally limited to a thin boundary layer in these high speed flows, the main flow can be considered isentropic. In this case pressure, density, and temperature are related as

$$p \propto \rho^\gamma \propto T^{\frac{\gamma}{\gamma-1}}. \quad (1)$$

During a fast isentropic expansion in a nozzle, a gas containing condensable vapours accelerates to supersonic velocity, and the temperature of the mixture drops with a very high cooling rate (10^4 - 10^6 K/s). A super-cooled non-equilibrium state is attained, in which no condensation has yet taken place. This metastable state does not last long. At some point in the supersonic part of the nozzle, nuclei of vapour molecules will spontaneously form. The nucleation rate becomes very high, and a large number of very small droplets, typically the size of a few nanometers, are almost instantaneously formed. Because of the very high concentration of small droplets ($>10^{15} \text{ m}^{-3}$), foreign particles acting as nucleation sites play no role in this condensation process; it is therefore considered a homogeneous condensation process. A process were

vapour condenses on foreign particles or solid walls is addressed to as a heterogeneous condensation process.

As the vapour mixture is still super-cooled (or super-saturated) these small nuclei will grow to form droplets. The vapour then depletes and returns to the equilibrium or saturated state.

The research into supersonic condensing flows started in the 1930's with the use of supersonic wind tunnels. Condensation in expanding nozzle flows has been studied extensively and this work continues today (e.g. see the work of the groups of Professor Wyslouzil at Ohio State University in the US and Professor Strey at the University of Cologne in Germany, see Khan *et al.* (2003)).

The feed stream in regular phase separators is typically a two-phase mixture. The dispersed phase being liquid droplets, bubbles or solid particles can be separated using the inertia of the heavier phase but generally no phase transition occurs in these devices. In a Twister device the feed stream is generally a single phase fluid containing a large number of components. The process of supersonic expansion and subsequent condensation of the vapour is used to create the second phase - being liquid droplets in the sub-micron range.

Figure 1 shows an artist impression of the Twister tube. The natural gas entering from the left is led over an innerbody with swirl imparting vanes in an annulus at the maximum width of the inner body. The inner body then contracts and due to the preservation of angular momentum the tangential flow increases dramatically. As the tangential velocity increases with the reduction of the inner body diameter, the axial velocity component is also increased by the shape of the outer contour resembling a supersonic nozzle contour. The resulting low temperature of the gas initiates the condensation process, and due to the extremely high rotational forces ($> 500,000$ times gravitational acceleration), the small droplets are driven towards the outside wall of the tube. A simple vortex finder then separates the dry core flow from the liquid and slip gas flowing along the wall. After separation occurs at the lowest temperature point in the Twister tube, the two streams are decelerated again in order to recover the kinetic energy in two concentric diffusers. In Figure 2 the process is plotted in a pressure temperature diagram. Starting at the boundary of the phase envelope at point A, the gas is expanded to point B at which point the separation occurs. After the separation, the gas is recompressed in the diffusers going towards point C at the outlets of the Twister device.

The typical conditions encountered inside a Twister tube pose a challenge for the CFD modelling. These being, the large range in velocity (Mach number ranges from 0.1 to 1.8), pressure (1-250 bar), and temperature (-70 – 40 C). On top of these challenges, the gas/vapour mixture (typically natural gas) is a multi-component, real gas mixture undergoing phase transition. The large swirl, with tangential velocities approaching sonic speeds, requires extra attention in the turbulence modelling. For the CFD modelling Twister BV has been using the commercial CFD package ANSYS CFX for the fluid dynamical modelling (Jones *et al.*, 2003).

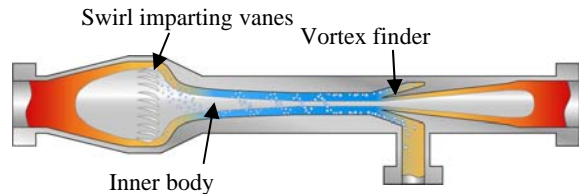


Figure 1: Artist impression of the Twister™ device. The flow direction is from left to right. The dry gas is continuing to the right. The separated liquid and slip gas are transported towards the bottom.

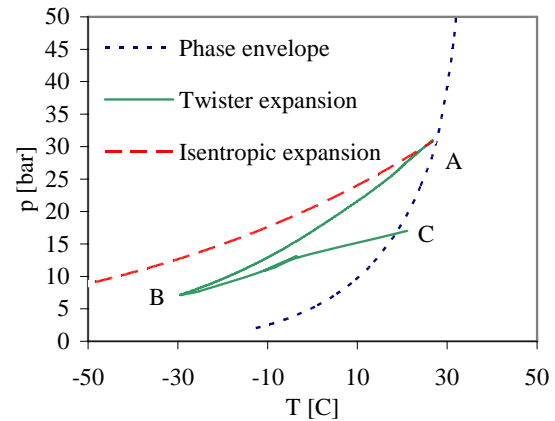


Figure 2: The Twister expansion and recompression trajectory in a P,T diagram plotted in combination with the phase envelope and an isentropic expansion.

TWISTER MODELING

The physical modelling of the Twister device can be divided in 3 parts:

- A hydrodynamic part, solving the flow field (RANS) with an appropriate turbulence model.
- A thermodynamic part, using the proper real gas mixture properties. This includes effects such as Joule-Thomson cooling (which is a typical real gas effect) and the effects of latent heat release due to condensation.
- A multi-phase and phase transition part. Here the slip between phases is accounted for as well as the conservation of mass species.

Solving the flow field

The flow in Twister is an internal annular flow. Typical length scales are the distance between the inner body and the outer body (2 cm height of the annulus), the length scale is in the axial direction (0.5-1 m from the vanes to the vortex finder). The Reynolds number characterising this flow field is approximately 10^7 .

In Figure 3 the streamlines originating from the inlet are depicted. The strong curvature of the flow lines demands a more complex turbulence model. The SSG Reynolds Stress Model from Speziale, Sarkar, and Gatski (1991) as implemented in CFX 10 is applied by default.

In order to minimise the lead time for a Twister design using CFD, the symmetry in the geometry is used to reduce the flow domain. This allows shorter CFD run-times while maintaining the proper grid resolution. A pie slice is selected between two inlet guide vanes. The grid applied in these reduced geometry CFD runs is shown in Figure 4. The velocity components in the axial and tangential directions resulting from a CFD run using a reduced geometry model are shown in Figure 5. The

depicted flow field in the annulus between inner and outer body starts at the end of the swirl imparting vanes and ends just after the vortex finder.

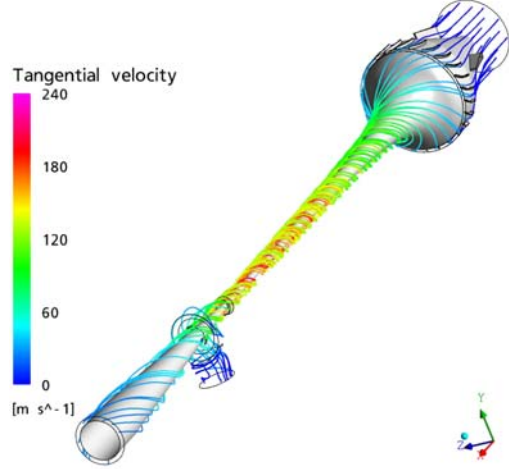


Figure 3: Streamlines in a Twister™ device coloured with the tangential velocity. Flow direction is from top-right to bottom-left.

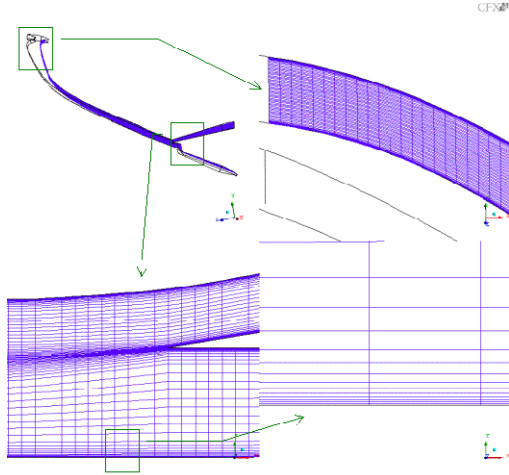


Figure 4: The grid as applied in the CFD runs on a pie section of the Twister™ tube showing the refinement of the grid near the walls in the boundary layer.

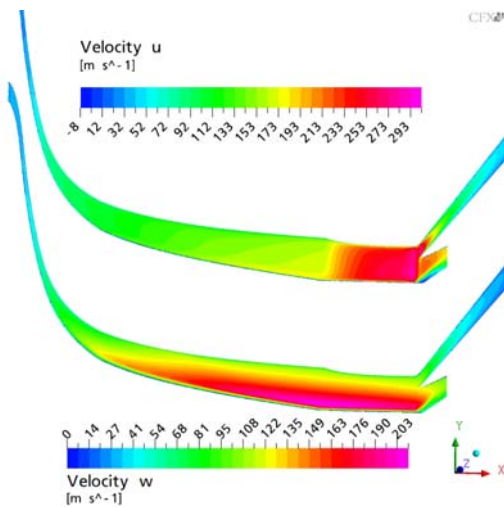


Figure 5: The axial (top) and tangential (bottom) velocities plotted in the reduced geometry. The axial

coordinate is scaled by a factor of 0.5 to enhance the interpretation of this picture.

Homogeneous nucleation and droplet growth

An important parameter for the condensation process is the saturation ratio S defined in a multi-component mixture as the ratio of actual molar fraction of component k in the vapour phase and the equilibrium molar fraction.

$$S_k = \frac{y_{vk}}{y_{eqvk}} \quad (2)$$

When S is larger than unity, condensation can occur. In the absence of foreign particles (e.g. dust) or solid surfaces the condensation process has to first overcome an energy barrier first, related to the formation of the surface of the nucleus or a cluster of vapour molecules. The rate, at which stable clusters are formed (which have overcome this energy barrier per unit time and volume), is called the homogeneous nucleation rate. This is a statistical process. The size of a nucleus at the top of this energy barrier (larger nuclei are stable and will continue to grow) is according to the classical nucleation theory defined as:

$$r^* = \frac{2\sigma}{\rho_L R_v T \ln(S)} \quad (3)$$

This cluster size is also referred to as the critical radius. Several expressions for the nucleation rate are available and the search for better theories is a continuous process (for an overview see Kashchiev, 2000 and for the latest developments see the article of Kalikmanov, 2006). For the work described here, the Internally Consistent Classical Theory (ICCT) from Girshick and Chiu (1990) was used. In principle, this is a single component nucleation theory as accurate multi-component nucleation theories are not yet available. In our approach, a single component is selected as the effective nucleating component. All other components are allowed to grow on these clusters or droplets. The expression for the nucleation rate is

$$J_{ICCT} = \frac{1}{S} \left(\frac{m_v}{\rho_L} \right) \sqrt{\frac{2\sigma}{\pi m_v}} \left(\frac{\rho_v}{m_v} \right)^2 \exp\left(\tau - \frac{4\tau^3}{27 \ln^2(S)} \right) \quad (4)$$

where

$$\tau = \frac{\sigma(36\pi)^{\frac{1}{3}} \left(\frac{m_v}{\rho_L} \right)^{\frac{2}{3}}}{k_B T} \quad (5)$$

The expression for the nucleation rate shows the strong dependency on properties as equilibrium fractions (via S) and the surface tension σ . A small change in the surface tension can change the nucleation rate by several orders of magnitude.

Droplet growth

As the majority of our applications use high pressure natural gas, the droplet growth is governed by diffusion. Expression for the change in droplet size over time is represented here by a summation of the individual contributions of all components

$$\left(\frac{dr^2}{dt} \right) = \sum_{k=1}^{N_{comp}} n_{vk} \left(\frac{Nu_{mk} D_k W_k}{\rho_{Lk}} \right) (y_k - y_{eqk}) \quad (6)$$

The droplets are assumed to be spherical and homogeneous (all components well mixed). For our high pressure applications, we can assume the droplet temperature to be equal to the surrounding gas temperature. The Nusselt number for mass transfer, Nu_m , is assumed constant (with a value of 2). More complex models including effects of kinetic growth (for large Knudsen numbers), droplet temperature or layered growth can also be applied if necessary. For a more detailed description of the droplet growth model the reader is referred to the work of Gyarmathy (1982) and Young (2001).

In Figure 6 and Figure 7 examples of a pressure and temperature profile with a corresponding nucleation rate and average droplet size are presented.

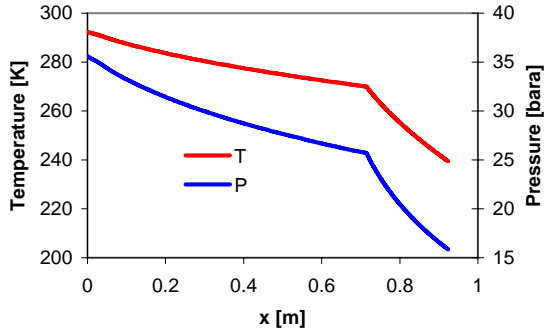


Figure 6: An example of the pressure and temperature profile in a Twister device. This result is obtained using a quasi one-dimensional model of the expansion inside a Twister tube. The location $x=0$ coincides with the end of the swirl imparting vanes.

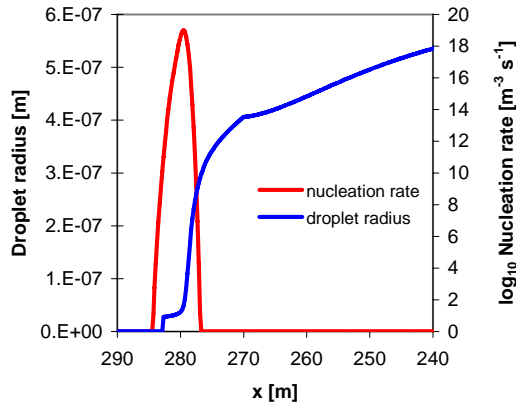


Figure 7: An example of the nucleation rate and droplet size as a function of temperature. This result is obtained using a quasi one-dimensional model of the expansion inside a Twister tube.

CFX implementation

The CFX implementation of the multi-component phase transition with interphase slip follows the approach from Jones (2003). The implementation is done as a single fluid comprising a mixture of vapour and liquid components with a single component as constraint. The Algebraic Slip Model (ASM) accounts for phase separation where drift velocity (u_d) is added to the convective velocity based on the drag relation for the droplets. As the ASM is only available for mass fractions (Y_k), all equations have to be

implemented as mass fraction equations. These equations are defined in the CFX manual. Disregarding the averaging notation, this is given by:

$$\frac{\partial}{\partial t} \rho Y_k + \frac{\partial}{\partial x_j} \rho (u_j + u_{dj}) Y_k = \quad (7)$$

$$\frac{\partial}{\partial x_j} \left(\Gamma_k + \frac{\mu_t}{Sc_t} \right) \frac{\partial}{\partial x_j} Y_k + Source_k$$

When we disregard the influence of the turbulent and diffusive fluxes (first term on the RHS of equation 7), equation 7 can be written for the vapour and liquid components as

$$\frac{D}{Dt} \rho Y_{vk} = -Source_k \quad (8)$$

$$\frac{D}{Dt} \rho Y_{Lk} = Source_k \quad (9)$$

Instead of solving for the droplet number density, we solve for a droplet mass fraction Y_{nN} in which each droplet is represented by a single molecule, with $m_n = W_n / N_A$. In principle the approach described here allows for more than one nucleating component. For each monodisperse droplet cloud originating from a nucleating component the equation:

$$\frac{D}{Dt} \rho Y_{nN} = m_n J \quad (10)$$

is solved. The term Y_{nN}/m_n now represents a droplet number density.

The source terms are now given by

$$Source_k = \frac{4}{3} \pi r^{*3} \rho_{Ln} J \delta_{nk} + \frac{\rho Y_{nN}}{m_n} 4 \pi \bar{r}^2 \rho_{Lk} \left(\frac{dr}{dt}(\bar{r}) \right) \quad (11)$$

In contrast to the approach described by Jones (2003) the MUSIG model is not used to limit the number of equations to be solved. This extension can easily be made but considerably increases the lead time for a Twister tube design. For validation purposes this extension will be investigated and compared to the monodisperse approach in the future.

RESULTS

In this section the results of a CFD run (using the model as described in the previous section) are presented. The velocity field was already shown in Figure 5, but in Figure 8 the corresponding temperature and pressure field is presented.

The strong increase in tangential velocity near the centre of the Twister tube is reflected in the decrease in temperature and pressure at that position. In Figure 9 the nucleation rate and resulting droplet number density are depicted. A first nucleation peak is located in the section of the Twister where a low expansion rate exists. In the second faster expanding section of the Twister tube the droplet growth is too slow to deplete the vapour, causing the saturation ratio to increase and a second nucleation peak occurs generating smaller droplets.

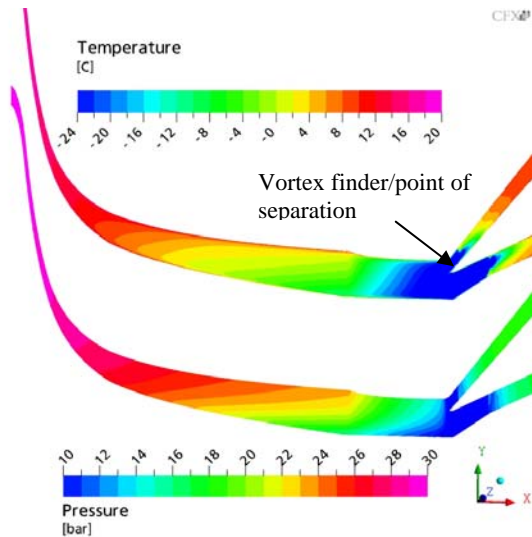


Figure 8: Pressure and temperature field from CFD in a Twister.

This sudden decrease in average droplet size due to the second nucleation peak can be seen in Figure 10 where the average droplet size and slip velocity is shown. In reality no droplets are present upstream of the nucleation peak but for numerical reasons (some parameters are droplet size dependent, such as growth) a droplet size is still assigned. This does not affect the results further downstream. The smaller average droplet size due to the second nucleation peak results in a lower slip velocity. This would argue for a model incorporating a size distribution as larger droplets in this case would still be separated despite the simultaneous formation of new smaller droplets.

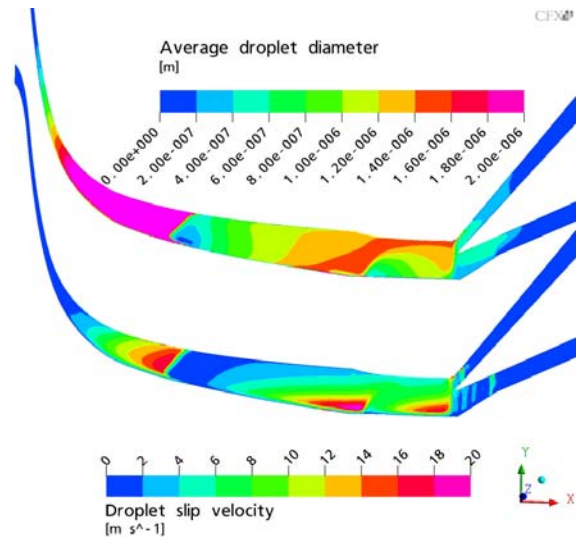


Figure 10: Droplet size and droplet slip velocity field from CFD in a Twister.

The actual separation on a mixture component level can be seen in Figure 11. Here the normalised total mass fraction (liquid and vapour fraction of one component normalised with the component vapour inlet mass fraction) is plotted for a light alkane (C_5 , pentane) compared with values for a heavy alkane (C_8 , octane). A value larger than unity indicates local enrichment of that particular component with respect to the Twister inlet flow.

Due to the lower partial vapour pressure octane will condense at a higher temperature. Condensation at a higher temperature (i.e. more upstream) results in an increased separation efficiency.

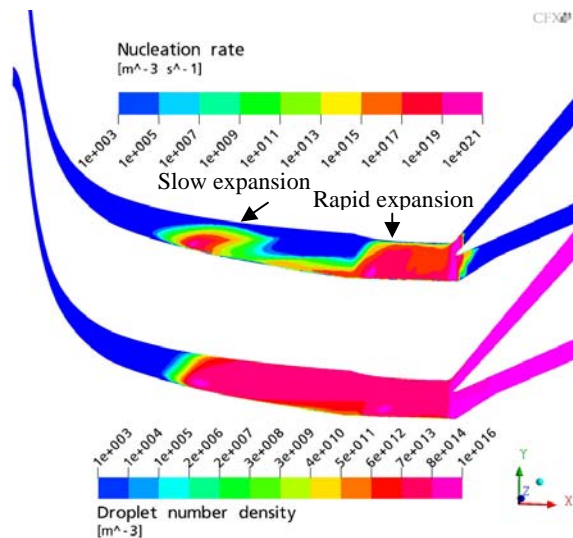


Figure 9: Nucleation rate and droplet number density field from CFD in a Twister.

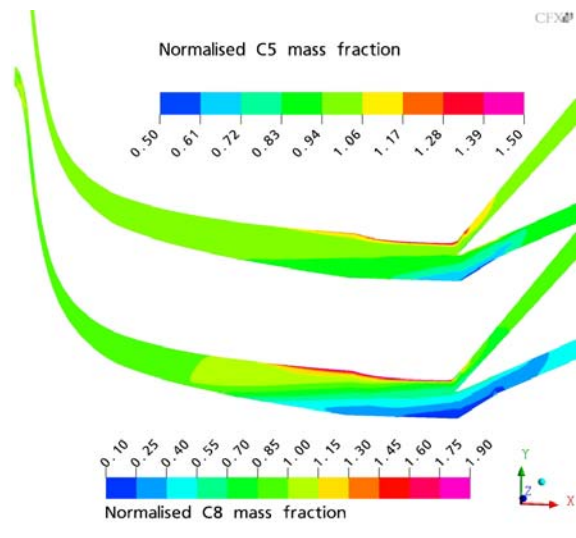


Figure 11: C_5 and C_8 recovery fields from CFD compared in a Twister. The total mass fraction (liquid and vapour) is normalised with the inlet vapour mass fraction.

Several configurations of the Twister™ device have been tested by Twister BV during 2005 and 2006 in order to validate the models as used in the CFD software. In Table 1 the experimental recoveries (vapour fraction at the dry gas outlet of the Twister tube divided by the inlet vapour fraction) are presented for both the CFD results as the

experimental values obtained by gas chromatograph analysis. Figure 12 is a graphical representation of these values based on the molecular weight of the components. In order to decrease the number of mass species equations solved in CFD (2 for each component for the liquid and vapour phase), components are lumped together for the CFD run.

For validation of the simulated flow field the pressure profiles obtained from the CFD results are compared with experimental pressure point readings from the same experiments in Figure 13.

| | mole weight | Recovery CFD |
|--|-------------|--------------|
| Lumped C ₁ - | 18.10 | -1.7% |
| Lumped C ₂ + C ₃ | 31.79 | 0.2% |
| Lumped C ₄ + C ₅ | 71.14 | 20.2% |
| Lumped C ₆ + C ₇ | 86.90 | 44.9% |
| C ₈ | 114.22 | 62.1% |
| Lumped C ₉ + | 130.19 | 66.1% |
| | | |
| | mole weight | Recovery EXP |
| CH ₄ | 16.04 | -1.02% |
| N ₂ | 28.01 | -0.5% |
| C ₂ H ₆ | 30.07 | 0.2% |
| CO ₂ | 44.01 | -0.7% |
| C ₃ H ₈ | 44.09 | 3.7% |
| i-C ₄ H ₁₀ | 58.12 | 8.7% |
| n-C ₄ H ₁₀ | 58.12 | 11.9% |
| DiMeth | 72.15 | 22.2% |
| i-C ₅ H ₁₂ | 72.15 | 28.7% |
| n-C ₅ H ₁₂ | 72.15 | 25.5% |
| C ₆ + | 86.17 | 65.4% |

Table 1: Component recoveries from testing (determined by gas-chromatograph on inlet and dry gas outlet) compared to CFD generated values.

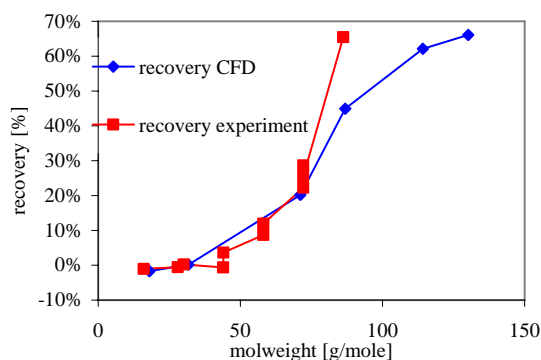


Figure 12: Experimental component recovery in Twister compared to the CFD results from Table 1.

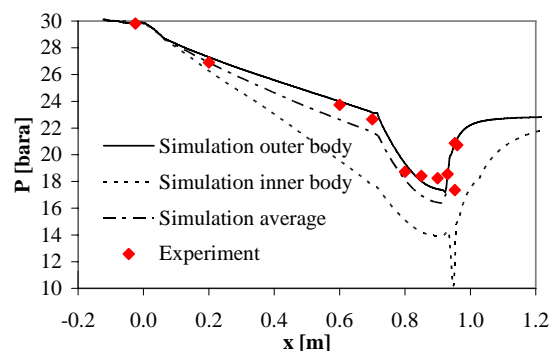


Figure 13: Experimental pressure profile compared to the CFD results in a Twister. The location $x=0$ coincides with the end of the swirl imparting vanes.

CONCLUSION

In this paper, we described the CFD model used to evaluate Twister designs. A multi-component real gas mixture, with phase transition based on non-equilibrium homogeneous nucleation, can be simulated. The first results of this model are compared with experimental values for both component recoveries and wall pressures. The component recovery shows the proper physical behaviour where heavy hydrocarbons will condense earlier and will have an increased recovery over light components. The comparison of the pressure profile gives a good indication on whether the flow field is simulated properly.

As the model is being continuously improved and more experimental data will be available in the future, a better understanding of the process in Twister will be achieved.

REFERENCES

- JONES, I.P., GUILBERT P.W., OWENS, M.P., HAMILL, I.S., MONTAVON, C.A., PENROSE, J.M.T., PRAST, B., (2003), "The use of coupled solvers for complex multi-phase and reacting flows", The 3rd International Conference on CFD in the Minerals and Process Industries, CSIRO, Melbourne, Australia, 10-12 December.
- KHAN, A., HEATH, C.H., DIEREGSWEILER, U.M., WYSLOUZIL, B.E., AND STREY, R., (2003), "Homogeneous nucleation rates for D2O in a supersonic Laval nozzle", *J. Chem. Phys.*, 119, 3138.
- SPEZIALE, C.G., SARKAR, S. AND GATSKI, T.B., (1991), "Modelling the pressure-strain correlation of turbulence: an invariant dynamical systems approach", *J. Fluid Mechanics*, Vol. 277, pp. 245-272.
- KALIKMANOV, V.I., (2006), "Mean-field kinetic nucleation theory", *J. Chem. Phys.*, 124, 124505.
- KASHCHIEV, D., (2000), "Nucleation; Basic Theory with Applications", Butterworth-Heinemann, Oxford.
- GIRSHICK, S., CHIU, C.-P., (1990), *J. Chem. Phys.*, 93, 1273.
- GYARMATHY, G., (1982), "The spherical droplet in gaseous carrier streams: review and synthesis", *Multiphase Science and technology*, volume 1, 99-279, Springer, Berlin.
- YOUNG, J.B., (2001), *Int. J. Heat Mass Transfer*, 44, 181.